Physical properties of $FeSe_{0.5}Te_{0.5}$ single crystals grown under different conditions

V. Tsurkan[1,2,a], J. Deisenhofer[1], A. Günther[1], Ch. Kant[1], M. Klemm[3], H.-A. Krug von Nidda[1], F. Schrettle[1], and A. Loidl[1]

[1] Experimental Physics 5, Center for Electronic Correlations and Magnetism, Institute of Physics, University of Augsburg, 86159 Augsburg, Germany
[2] Institute of Applied Physics, Academy of Sciences of Moldova, MD 2028, Chisinau, Republic of Moldova
[3] Experimental Physics 2, Institute of Physics, University of Augsburg, 86159 Augsburg, Germany

Abstract. We report on structural, magnetic, conductivity, and thermodynamic studies of $FeSe_{0.5}Te_{0.5}$ single crystals grown by self-flux and Bridgman methods. The lowest values of the susceptibility in the normal state, the highest transition temperature T_c of 14.4 K, and the largest heat-capacity anomaly at T_c were obtained for pure (oxygen-free) samples. The critical current density j_c of 8.6×10^4 A/cm^2 (at 2 K) achieved in pure samples is attributed to intrinsic inhomogeneity due to disorder at the anion sites. The samples containing an impurity phase of Fe_3O_4 show increased j_c up to 2.3×10^5 A/cm^2 due to additional pinning centers. The upper critical field H_{c2} of ∼500 kOe is estimated from the resistivity study in magnetic fields parallel to the c-axis using a criterion of a 50% drop of the normal state resistivity R_n. The anisotropy of the upper critical field $\gamma_{H_{c2}} = H_{c2}^{ab}/H_{c2}^{c}$ reaches a value ∼6 at $T \longrightarrow T_c$. Extremely low values of the residual Sommerfeld coefficient γ_r of about 1 mJ/mol K^2, compared to the normal state Sommerfeld coefficient $\gamma_n = 25$ mJ/mol K^2 for pure samples indicate a high volume fraction of the superconducting phase (up to 97%). The electronic contribution to the specific heat in the superconducting state is well described within a single-band BCS model with a temperature dependent gap $\Delta(0\ \mathrm{K}) = 27(1)$ K. A broad cusp-like anomaly in the electronic specific heat observed at low temperatures in samples with suppressed bulk superconductivity is ascribed to a splitting of the ground state of the Fe^{2+} ions at the 2c sites. This contribution is fully suppressed in the ordered state in samples with bulk superconductivity.

1 Introduction

The recent finding of high-temperature superconductivity in iron pnictides [1–3] and iron chalcogenides [4] inspired an immense research activity in complex materials similar to the discovery of high-T_c cuprate superconductors two decades ago. Among the new iron-based superconductors, the iron chalcogenides are of particular interest due to a simple crystal structure (Fig. 1). It consists of Fe ions tetrahedrally coordinated by Se and Te arranged in layers stacked along the c-axis in the tetragonal lattice without any other interlayer cations, as for example in pnictides. Therefore, the iron chalcogenides were believed to be most suitable for investigation of the interplay of competing orders and pairing mechanisms. However, recently it was recognized in Fe(Se, Te) that Fe ions can occupy also the 2c positions in the anion plane [5,6].

Nearly stoichiometric FeSe becomes superconducting below 8 K at ambient pressure [4] but the transition temperature can be enhanced up to 37 K by application of external pressure [7,8]. The superconducting properties of FeSe were shown to be extremely sensitive to deviations from the stoichiometry [9,10]. The substitution of Se by Te in FeSe increases the temperature of the superconducting

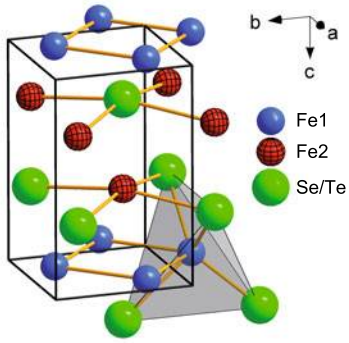

Fig. 1. (Color online) Crystal structure of $FeSe_{0.5}Te_{0.5}$ demonstrating the tetrahedral coordination of Fe1 ions in 2a positions (blue spheres) by anions of Se and Te (green spheres) and Fe2 ions in 2c position (red spheres) in the anion plane.

[a] e-mail: vladimir.tsurkan@physik.uni-augsburg.de

transition to a maximum of about 14 K for 50% of replacement [11,12]. The intrinsic disorder due to random distribution of the Se and Te ions among the anion sites in the crystal lattice is expected to reduce the sensitivity of FeSe to non-stoichiometry. Subsequently, several authors recently reported on the successful preparation of high quality single crystals of $FeSe_{1-x}Te_x$ using Bridgman [13–15] and flux methods [16,17]. The existing data show large variations in magnetic and conducting behavior of Fe-Se(Te) obviously related to differences in the growth conditions and purity of the starting materials. Hence, only little information about the intrinsic properties of $FeSe_{0.5}Te_{0.5}$ is available so far.

Here we report on the magnetic susceptibility, resistivity and heat-capacity measurements of $FeSe_{1-x}Te_x$ with nominal concentration $x = 0.5$. The samples were prepared in various ways and exhibit significantly different behavior which was investigated in the temperature range 2–400 K and in external magnetic fields up to 140 kOe.

2 Experimental

Single crystals of $FeSe_{0.5}Te_{0.5}$ were grown by self-flux and Bridgman methods. Chips and shots of high-purity elements, 99.98% Fe, 99.999% Se, and 99.999% Te, were used in the growth experiments. To get a minimal amount of oxide impurity we additionally purified Se (for growth runs F216) and Te (for growth runs F213 and F216) by zone melting. Handling of these samples was done in an argon box with residual oxygen and water content less than 1 ppm. The growth of single crystals was performed in evacuated double quartz ampoules. For different runs in the self-flux method the soaking temperature varied between 900 and 1100 °C. The cooling rate varied between 1 and 60 °C/h. In the Bridgman method we used pulling rates between 0.5 and 2 mm/h and rotation speed of 2–5 turns/min. Final treatment of the samples in both preparation methods was done at 410 °C for 70–100 h followed by quenching in ice water. The plate-like samples with shiny faces with dimensions $\sim 3 \times 5$ mm^2 in the *ab* plane and thickness up to 0.5 mm along the *c* axis were obtained on the top of the solidified ingot. The single-crystallinity of the grown samples was checked by the single crystal X-ray diffraction. The sample composition was investigated by energy dispersive X-ray (EDX) analysis using INCA system (Oxford Instruments). The phase content of the samples was analyzed by X-ray powder diffraction (CuK_α radiation, $\lambda = 1.540560$ Å) on crushed single crystals using a STADI-P powder diffractometer (STOE & CIE) with a position sensitive detector.

The magnetic measurements were performed in a temperature range 2–400 K and in magnetic fields up to 50 kOe using a SQUID magnetometer MPMS 5 (Quantum Design). Electron-spin resonance (ESR) measurements were performed in a Bruker ELEXSYS E500 CW spectrometer at X-band frequencies (9.36 GHz) equipped with a continuous He gas-flow cryostat in the temperature region $4.2 \leq T \leq 300$ K. The heat capacity was measured by a relaxation method using a Quantum Design physical properties measurement system (PPMS) in a temperature range 1.8–300 K and magnetic fields up to 90 kOe. The magnetic field was applied parallel to the *c*-axis of the samples. The resistivity studies were done on rectangular samples by a four-point method in the temperature range 2–300 K and in magnetic fields up to 140 kOe using a He-flow cryostat (Oxford Instruments) and using the resistivity measurement option of the PPMS in magnetic fields up to 90 kOe. The contacts were made by conductive silver paint.

3 Experimental results and discussion

3.1 EDX and X-ray analysis

The preparation conditions and the EDX data are presented in Table 1. The EDX measurements on samples from various growth experiments provide no indication that the different methods used for the crystal growth yield different compositions. No significant gradient in the Te/Se ratio along the sample was observed. The observed maximal deviations of Se/Te ratio for some samples were of about 10% from the nominal 50/50% composition. The ratio Fe/(Se+Te) in the samples was deviating about 2% from the stoichiometric value indicating a low content of excess iron. The X-ray diffraction patterns for the samples under investigation (Fig. 2a) are consistent with tetragonal symmetry P4/nmm for the main $FeSe_{0.5}Te_{0.5}$ phase and with hexagonal symmetry P63/mmc for the impurity phase Fe_7Se_8. The refinement was performed using the FULLPROF SUITE [18]. The results of the refinement for one of the samples are shown in Figure 2b. The occupation of Te and Se at the 2c sites was refined constraining their sum to unity. A similar constraint was used for the occupation of Fe ions for the main phase allowing for two different sites (2a and 2c). The results of the Rietveld refinement for different samples are given in Table 2. The refined occupation factors for Te and Se ions for the main tetragonal phase are in general agreement with the EDX data. The occupation of iron an the 2c sites was ∼6–9%. The values of the lattice parameters for different samples varied within the range 3.800–3.803 Å for the *a(b)* lattice constant, and between 6.026–6.047 Å for the *c* parameter and are close to those reported in reference [13] for single crystals of similar composition.

Figure 3 shows the morphology of the as-grown oxygen-free samples within the *ab*-plane (upper panel) and along the *c*-axis (lower panel) as revealed by scanning-electron microscope. Large flat regions are clearly seen in the *ab*-plane without distinct domains with different orientation. The apparent domains on the upper picture represent the fragments of subsequent layers (after cleaving procedure) which are stacked along the *c*-axis as shown in the lower panel of this figure. The structure of the samples along the *c*-axis consists of a set of extremely thin sheets with excellent crystallinity and without visible inclusions of foreign phases. Using higher magnification we estimated the thickness of these sheets to be below 100 nanometers

Table 1. Preparation conditions and EDX data for $FeSe_{0.5}Te_{0.5}$ samples.

Sample	Preparation conditions				Concentration			Average over
	Method	Soaking temperature	Soaking time	Cooling rate	Fe	Se	Te	
Br N5	Bridgman	1084 °C	24 h	0.5 mm/h	0.978(10) 0.958(10)	0.498(10) 0.496(8)	0.502(10) 0.504(6)	35 points area 1.2×0.9 mm^2
F213	self-flux	1100 °C	72 h	60 °C/h	0.978(10)	0.439(8)	0.561(6)	area 0.5×0.7 mm^2
F216 step 1	self-flux	1100 °C	72 h	60 °C/h	0.992(10) 0.974(8)	0.469(9) 0.488(6)	0.539(9) 0.536(4)	10 points area 0.5×0.3 mm^2
F216 step 2	self-flux	1100 °C	72 h	1 °C/h	1.015(10) 1.013 (8)	0.491(9) 0.482(5)	0.493(9) 0.505(5)	5 points area 0.5×0.3 mm^2

Table 2. Structural data obtained from the Rietveld refinement for $FeSe_{0.5}Te_{0.5}$ samples.

Sample	Occupation				Lattice constant		Tetragonal phase	Hexagonal phase	R_{wp}	R_{exp}	χ^2
	Fe1 /2a/	Fe2 /2c/	Se /2c/	Te /2c/	a, b [Å]	c [Å]	[%]	[%]			
Br N5	0.907(3)	0.093(3)	0.48(1)	0.52(1)	3.8020(4)	6.0489(9)	94.5	5.5	3.53	2.48	2.02
F213	0.930(5)	0.070(5)	0.49(1)	0.51(1)	3.8011(2)	6.0409(7)	94.5	5.5	3.68	2.54	2.10
F216 step 1	0.929(3)	0.071(3)	0.49(1)	0.51(1)	3.8025(3)	6.0300(9)	98.6	1.4	3.0	2.36	1.62
F216 step 2	0.937(3)	0.063(3)	0.52(1)	0.48(1)	3.8000(3)	6.0257(8)	97.9	2.1	3.06	2.49	1.51

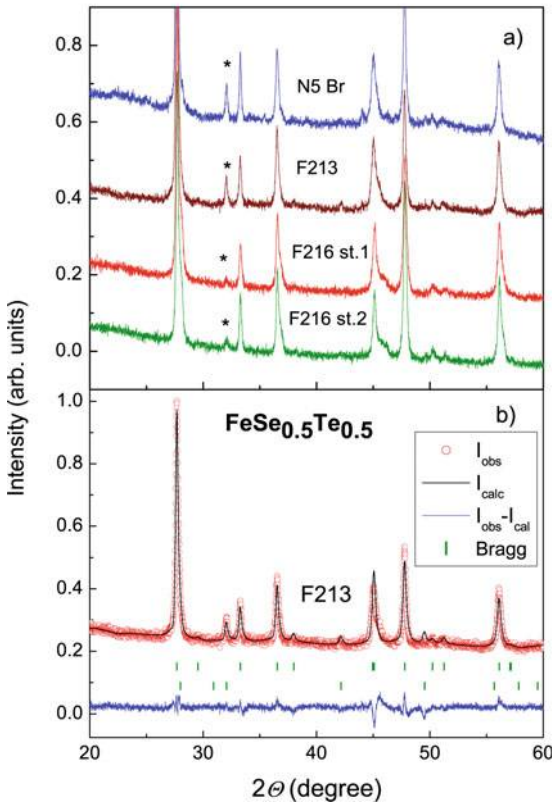

Fig. 2. (Color online) (a) Room temperature X-ray diffraction patterns for $FeSe_{0.5}Te_{0.5}$ samples prepared under different conditions. Stars indicate the impurity phase; (b) experimental (open circles) and refined (black line) X-ray diffraction patterns for sample F213. Blue line – difference between experimental and calculated intensities. Vertical lines mark Bragg positions: top row – main tetragonal phase; bottom – impurity hexagonal phase.

revealing a pronounced two dimensionality of our layered single-crystalline $FeSe_{0.5}Te_{0.5}$ samples.

3.2 Susceptibility and magnetic hysteresis

Figure 4a shows the temperature dependence of the magnetic susceptibility χ for samples from different growth runs measured on cooling in a field of 10 kOe applied parallel to the c-axis. The samples prepared from the non-purified Se and Te and handled in air have a relatively high susceptibility, $\sim(1\text{–}2) \times 10^{-2}$ emu/mol. Below 300 K the susceptibility continuously increases on decreasing temperature, then shows a pronounced downturn at 125 K and a clear anomaly at the superconducting transition at $T_c \sim 14$ K. The downturn at 125 K is related to the Verwey transition of Fe_3O_4 [19], which was also evidenced by electron-spin resonance and specific-heat measurements (see below). The electron-spin resonance spectra of the samples handled in air show broad features characteristic of the Verwey transition observed in magnetite Fe_3O_4 which was investigated complimentarily. Below the Verwey transition these features in the spectra fully disappear similar to the magnetite sample. The purest (oxygen-free) samples do not show any noticeable features related to the Verwey transition and the ESR experiment does not reveal any intrinsic absorption of localized moments.

Samples prepared from the purified elements and handled in the argon box have susceptibility values one order of magnitude lower and do not show any anomaly at 125 K, although the X-ray diffraction still evidences some amount of the impurity hexagonal phase (Tab. 2). The susceptibility of the purest oxygen-free sample, F216 step 1, prepared by fast cooling (1 °C/min) manifests a non-monotonous temperature behavior with a broad maximum at around 180 K. It also shows the

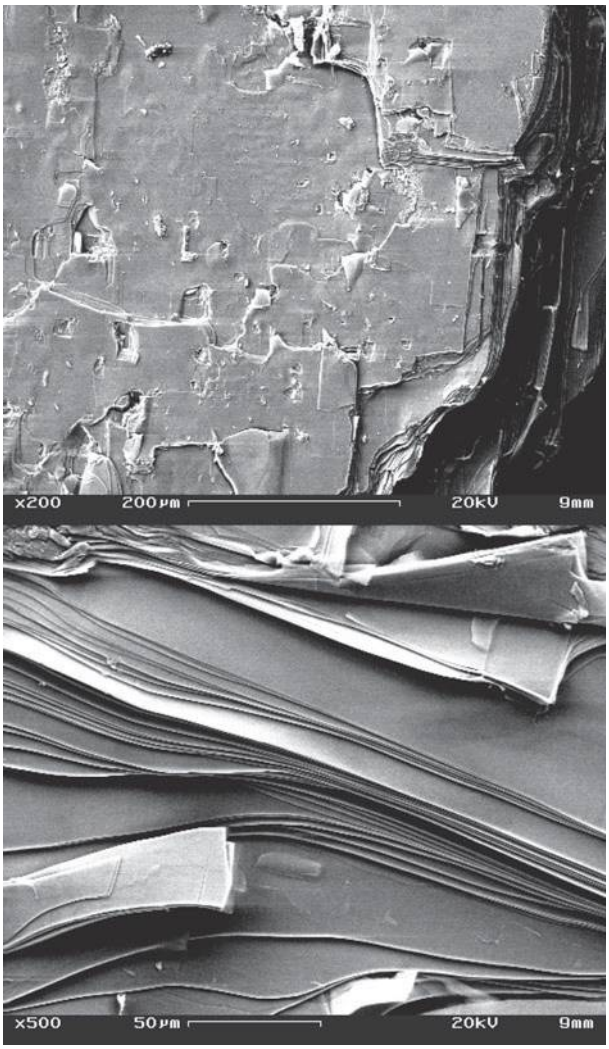

Fig. 3. Scanning-electron microscope images of the samples along the *ab*-plane (sample F213)-upper panel, and along the *c*-axis (sample F216 step 1)-lower panel.

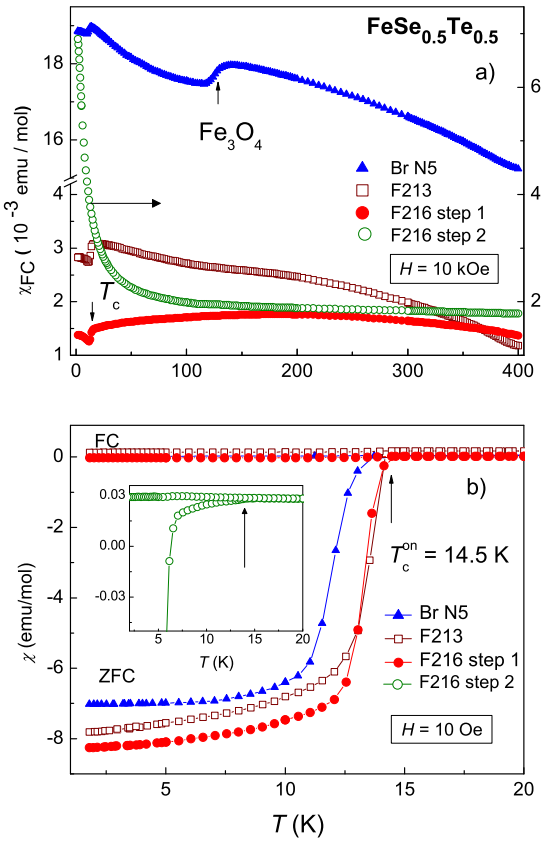

Fig. 4. (Color online) (a) Temperature dependence of the field-cooled susceptibility of $FeSe_{0.5}Te_{0.5}$ measured in a field of 10 kOe applied along the *c*-axis. The arrow at 125 K marks the anomaly related to Fe_3O_4; (b) temperature dependences of ZFC and FC susceptibilities of samples with bulk superconductivity measured in a field of 10 Oe applied along the *c*-axis. Arrow indicates the temperature of the onset of the superconducting transition $T_c^{on} = 14.4$ K for the purest samples. Inset: ZFC and FC susceptibilities of the sample with filamentary superconductivity shown on enlarged scale.

sharpest anomaly at around 14 K at the superconducting transition. Surprisingly, repeated melting of this sample followed by slow cooling with the rate of 1 °C/h, drastically changes the magnetic behavior. The susceptibility of this sample is temperature independent at high temperatures and shows a paramagnetic tail at low temperatures. An explanation of the low-temperature susceptibility tail in these poorly superconducting samples due to the hexagonal-phase can be excluded, because the amount of the hexagonal phase can be strongly reduced in the oxygen-free samples. The apparent effect of the hexagonal impurity on the susceptibility can be revealed by comparing the oxygen-free samples F213 and F216 step 1, containing respectively 5.5 and 1.4% of the hexagonal phase. The paramagnetic tail might be associated with localized iron ions. Recent investigations of FeSe(Te) samples with iron excess [6,17,20] established a localized magnetic iron moment at the 2c sites which can suppress superconductivity. However, both *well* and *poorly* superconducting samples contain comparable amount of the Fe ions at the 2c sites (Tab. 2). Estimating the concentration of the localized magnetic ions in the poorly superconducting samples using a Curie-Weiss fit in the temperature range 2–50 K (after subtraction of the constant temperature-independent contribution) yields a value of 6.5×10^{-3} per mol which is 10 times less than the concentration of the Fe ions at the 2c sites revealed by the Rietveld refinement and about 3 times less than the amount of the excess iron revealed by the EDX analysis in this sample (see Tab. 1). The rather low value of the Curie-Weiss temperature of 2 K can indeed suggest paramagnetic behavior. However, the reason why the paramagnetic tail is suppressed in samples with full bulk susceptibility is unclear at present and needs additional investigations. In any case, it seems unrealistic to associate the paramagnetic contribution with non-reacted Fe, because its amount (if present) in samples after the second step of preparation cannot be higher than after the first step.

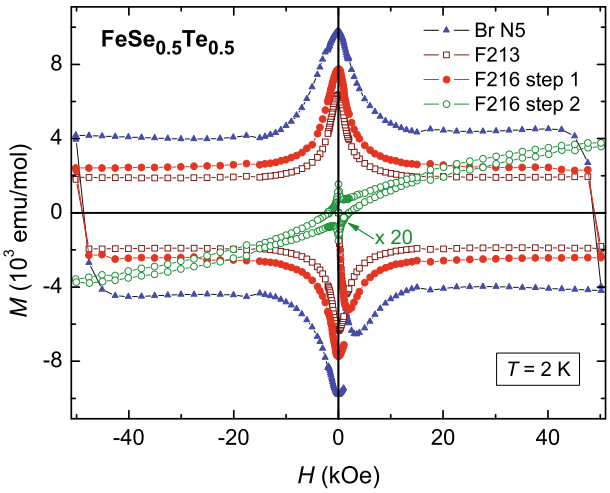

Fig. 5. (Color online) Hysteresis loops measured at 2 K with the magnetic field applied along the c-axis for different single crystalline $FeSe_{0.5}Te_{0.5}$ samples. The data for the slowly cooled sample are magnified by a factor of 20 for clarity.

Figure 4b shows the temperature dependence of the zero-field cooled (ZFC) and field-cooled (FC) susceptibility measured in a field of 10 Oe applied parallel to the c-axis. The measurements along the ab-plane showed similar results except that the diamagnetic response was substantially higher for the field parallel to the c-axis. The samples containing both, oxide and hexagonal-phase impurities manifest rather broad transitions into the superconducting state. At the same time, the temperature of the onset of the superconductivity, T_c^{on}, shows only a small change at around 13.5 K for these samples. We found the sharpest transition and, respectively, the highest T_c of 13.9 K (with T_c^{on} of 14.4 K) for samples grown from the purified elements under fast cooling conditions only. The values of $4\pi\chi$ at 2 K calculated from the data shown in Figure 4b are far above unity indicating that the low-field susceptibility of samples with high diamagnetic response is dominated by demagnetizing effects. The volume fraction of the superconducting phase was therefore estimated from χ_{ZFC} on needle-like crystals for the field applied along the ab-plane with the smallest demagnetizing factors and reached 98% for the purest samples. At the same time, in the poorly superconducting sample the onset of the transition remains at the same temperature as in well superconducting samples, but it is masked by a temperature independent paramagnetic background and, therefore, can be evidenced only on zooming the data as shown in the inset in Figure 4b. The volume fraction of the superconducting phase with T_c^{on} of 14.4 K in this sample is by more then two orders lower than in the well superconducting sample suggesting filamentary superconductivity.

Figure 5 presents the magnetization hysteresis loops for different samples measured at 2 K with the field applied along the c-axis. The hysteresis loops for samples with a high volume of the superconducting phase have a symmetric character which indicates dominant bulk pinning and small contribution of surface pinning [21]. Below the transition temperature the diamagnetic response in these samples dominates over the full measured field range. The samples containing oxide impurities show an enhanced (by $\sim$ 20%) magnetization compared to the oxygen-free samples due to additional pinning centers of Fe_3O_4. A strongly contrasting hysteretic behavior was observed for the oxygen-free samples prepared under slow-cooling conditions. These samples exhibit a width of the hysteresis loops reduced almost by two orders of magnitude suggesting full suppression of bulk superconductivity.

Surprisingly, such a drastic change of the magnetic properties of the sample with suppressed bulk superconductivity is not accompanied by notable changes in the structural data. The X-ray diffraction patterns of these samples show a comparable amount of the tetragonal and hexagonal impurity phases (Fig. 2a). Their refinement data (Tab. 2) do not reveal any essential variations of the site occupancy for the iron ions and for the anions as well as of the lattice parameters of the main tetragonal phase. Although any comparison of the low-temperature superconducting data and the X-ray diffraction data taken at room temperature is not plausible, our results indicate a rather subtle role of the structure which probably cannot be resolved using conventional X-ray facilities.

Figures 6a and b show, respectively, the magnetic hysteresis and critical current at different temperatures for the purest samples with bulk superconductivity. The critical current density was estimated from the width of the hysteresis loops using the Bean model for hard superconductors [22,23]. At 2 K the critical current density j_c at zero field reaches a value of 8.6×10^4 A/cm^2. For the sample grown by Bridgman method we obtained $j_c = 9.4 \times 10^4$ A/cm^2. For the sample grown from self-flux and intentionally oxidized after the first step we found nearly 3 times higher values of $j_c = 2.3 \times 10^5$ A/cm^2. Thus, the oxidation allows to increase the critical current. The critical current for the purest sample with high volume fraction of the superconducting phase decreases approximately three times in fields up to 20 kOe but then flattens at this level up to the largest measured fields suggesting a high current-carrying ability of the material. An estimation of critical currents for $T = 0$ from fits to the experimental data was performed using a generalized power-law dependence $j(T) = j(0)[1 - (T/T_c)^p]^n$, with $p = 0.5$, $n = 1.5$ and $T_c = 13.8$ K. The respective fit is shown by the dotted line in the inset of Figure 6b, yielding a value $j(0) = 1.7 \times 10^5$ A/cm^2. The calculated value of $j(0)$ is close to those determined for high-quality superconducting single crystals of $Ba(Fe_{1-x}Co_x)_2As_2$ [24]. Table 3 summarizes the critical current densities calculated from the hysteresis loops at 2 K together with the critical temperature T_c and lower critical field H_{c1} determined from the magnetic data.

3.3 Electrical resistivity

Figure 7a presents the temperature dependences of the resistivity for the investigated samples. The oxygen-free

Table 3. Superconducting parameters: transition temperature, critical current, upper and lower critical fields for $FeSe_{0.5}Te_{0.5}$ samples.

Sample	T_c^{on} (K)	j_c (kA/cm^2) (2 K)	j_c (kA/cm^2) (0 K)	H_{c1} (kOe) (2 K)	H_{c2} (kOe) $[H \parallel c]$	H_{c2} (kOe) $[H \parallel ab]$
Br N5	13.5	94	250	3	510/920*	850
F213	14.5	77		1.4	570/750*	
F216 step 1	14.4	86	170	1.2	490/980*	
F216 step 2	7.6	0.8		0.1		

* Estimated from the heat capacity measurements.

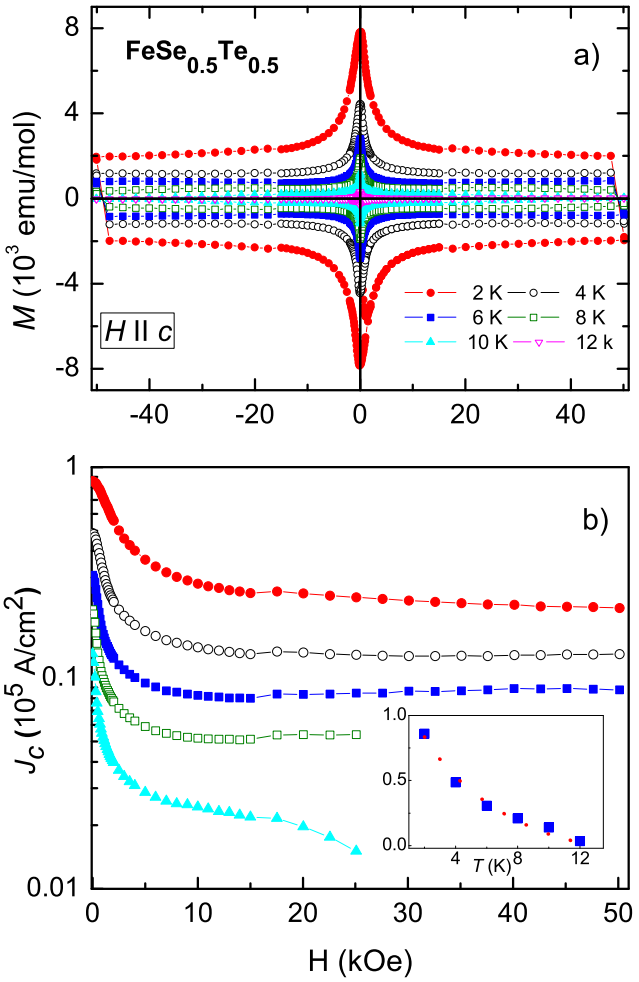

Fig. 6. (Color online) (a) Hysteresis loops at different temperatures measured for the field applied along the c-axis for $FeSe_{0.5}Te_{0.5}$ sample F216 step 1; (b) critical current density j_c vs. magnetic field at different temperatures for the same sample. The inset shows the temperature dependence of the critical current at zero field with the fit by the power law (dashed line).

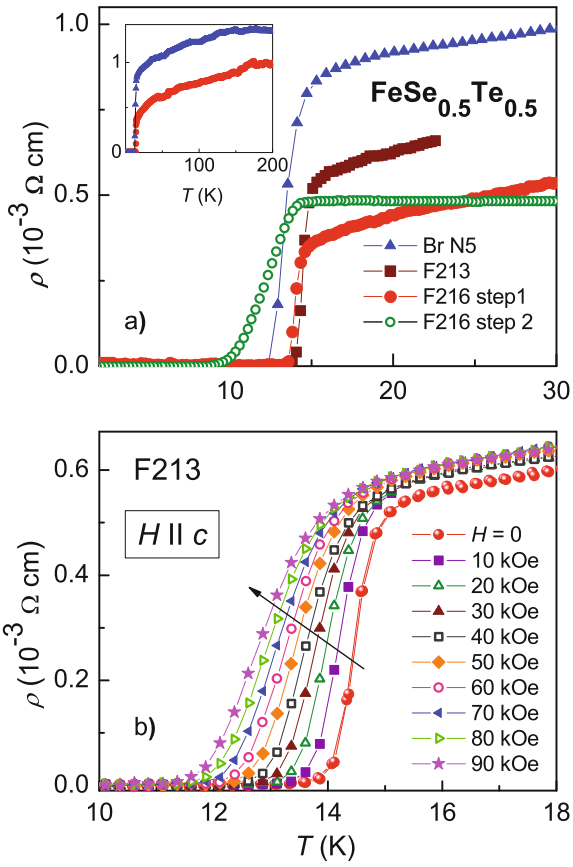

Fig. 7. (Color online) (a) Temperature dependences of the resistivity for different $FeSe_{0.5}Te_{0.5}$ samples measured on cooling in zero external magnetic field. Inset: temperature dependences of the resistivity for samples BrN5 and F216 step 1 measured up to 200 K; (b) temperature dependences of the in-plane resistivity for oxygen-free sample F213 measured at various magnetic fields applied parallel to the c-axis. The arrow shows the direction of increasing field.

samples have a lower value of the resistivity in the normal state compared to the samples with oxide impurity which can be attributed to increased scattering of charge carriers on additional impurity centers related to Fe_3O_4. The resistivity of samples with high volume fraction of the superconducting phase exhibits a metal-like temperature dependence below 200 K down to T_c as shown in the inset of this figure. Such a behavior was established earlier only for samples with a low amount of excess iron [20]. In contrast, the resistivity of samples with suppressed bulk superconductivity shows a temperature independent behavior at high temperatures down to T_c. The resistivity of these samples drops at approximately the same temperature as in the samples with high superconducting

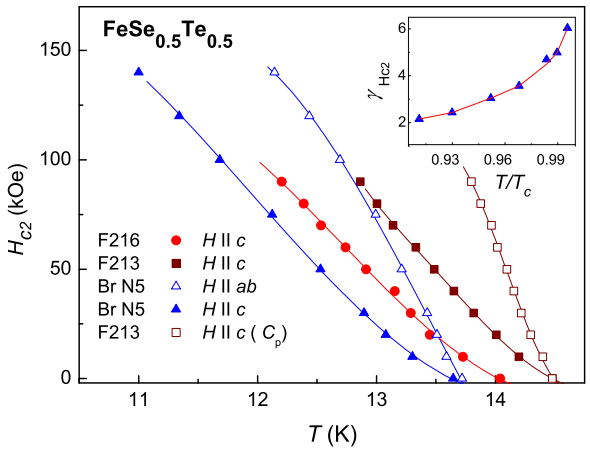

Fig. 8. (Color online) Temperature dependences of the upper critical field H_{c2} determined using the criterion of $0.5R_n$ for samples grown by different methods with magnetic field H parallel to the c-axis (closed symbols) and parallel to the ab-plane (open triangles). The open squares represent the data for sample F213 calculated from the specific heat (see text). The inset shows the temperature dependence of the anisotropy of the upper critical field $\gamma_{H_{c2}} = H_{c2}^{ab}/H_{c2}^{c}$ in the vicinity of T_c for sample Br N5.

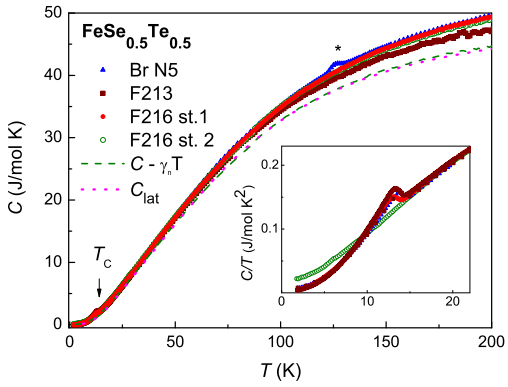

Fig. 9. (Color online) Temperature dependences of the specific heat for different samples. The star indicates the anomaly at the Verwey transition due to the presence of Fe_3O_4 impurity in sample Br N5. The dashed and dotted lines present the lattice specific heat as described in the text. The inset shows the specific heat in the representation C/T vs. T in the transition region.

parameters, but the resistive transition is strongly broadened and shifted to lower temperatures in agreement with the susceptibility data.

Figure 7b illustrates the effect of magnetic field on the in-plane resistivity in the transition region for one of the oxygen-free samples (F213). The field was applied parallel and perpendicular to the c-axis, and the measurements were done on warming after cooling in zero field. The resistivity curves are displaced to lower temperatures with increasing magnetic field with a stronger shift of the transition for the field parallel to the c-axis than for the perpendicular configuration. The obtained data are in general agreement with the respective results on the superconducting $FeSe_{1-x}Te_x$ samples with different x reported earlier [17,25].

In Figure 8 the temperature dependences of the upper critical field $H_{c2}(T)$ estimated using the criterion of a 50% drop of the normal state resistivity R_n are shown. The calculated data show a similar behavior for different samples with the shift on the temperature scale corresponding to a difference in their transition temperatures. On approaching T_c the slope of the $H_{c2}(T)$ curve for the configuration $H \parallel c$ becomes smaller compared to that of the lower temperatures. Contrary, the slope of $H_{c2}(T)$ for the configuration $H \perp c$ shows a slight increase on approaching T_c. The anisotropy of the upper critical field defined as $\gamma_{H_{c2}} = H_{c2}^{ab}/H_{c2}^{c}$ shows a notable increase on approaching T_c from $\gamma_{H_{c2}} = 2.15$ at $T/T_c = 0.91$ to $\gamma_{H_{c2}} = 3.6$ at $T/T_c = 0.968$ and finally reaches $\gamma_{H_{c2}} = 6$ at $T/T_c = 0.996$ (see inset of Fig. 8). This observation is in disagreement with the nearly isotropic behavior of the upper critical field reported by other studies on superconducting $FeSe(S)_{1-x}Te_x$ with different levels of substitution [17,25]. The higher anisotropy value of $\gamma_{H_{c2}}$ may reflect the better quality of our samples compared to earlier reports. The upper critical field $H_{c2}(0)$ for $T = 0$ K calculated within the Werthamer-Helfand-Hohenberg (WHH) model for conventional superconductors, defined by $H_{c2}(0) = -0.69T_c(dH_{c2}(T)/dT)\ |_{T_c}$ for a weak-coupling regime [26]. The results are presented in Table 3. The values of $H_{c2}(0)$ are rather similar for all samples, are independent of the impurity content, and vary in the range 490–570 kOe for the magnetic field parallel to the c-axis. $H_{c2}(0)$ for one of the samples measured along the ab-plane equals ~850 kOe. Such high values of $H_{c2}(0)$, which are far above the Pauli paramagnetic limit $H_p = 1.84T_c \sim 250$ kOe can be attributed to an enhanced impurity scattering from the Fe at 2c sites as proposed in reference [14].

3.4 Specific heat

Figure 9 shows the temperature dependences of the specific heat for samples with different superconducting properties. They exhibit a similar behavior and similar values of the specific heat at temperatures above 15 K. A small anomaly at 125 K is observed for sample Br N5 which contains Fe_3O_4. By scaling the entropy involved in this anomaly with that of the specific-heat anomaly at the Verwey transition measured in Fe_3O_4 we estimated the amount of the oxide impurity in this sample to be at a level of ~0.6 mol%. The inset in Figure 9 illustrates the specific heat in the representation C/T vs. T in the low temperature range. The samples with bulk superconductivity exhibit a pronounced anomaly at around 14 K. As the transition in the poorly superconducting sample is smeared out, no discernible anomaly in the specific heat could be detected. The data in Figure 9 indicate that the

Table 4. Parameters determined from the heat capacity measurements.

Sample	γ_r (mJ/mol K^2)	β (mJ/mol K^4)	γ_n (mJ/mol K^2)	Δ_0 (K)	$2\Delta_0/T_c$
Br N5	5.2	0.75	24	26.6	3.94
F213	0.82	0.85	25	28.1	3.86
F216 step 1	0.96	0.94	25	25.9	3.57
F216 step 2	19.3	0.90	23		

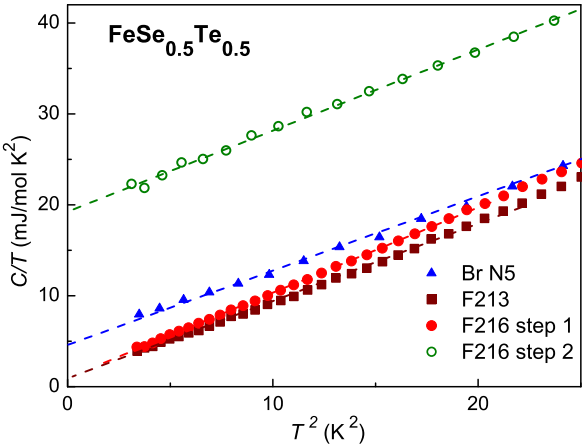

Fig. 10. (Color online) Temperature dependences of the specific heat in the representation C/T vs. T^2 for different samples.

superconducting contribution to the specific heat is small compared to that of the lattice contribution which dominates the total specific heat. Therefore, an accurate estimation of the lattice specific heat is extremely important for correct evaluation of the electronic specific heat and resulting superconducting parameters.

Figure 10 shows the temperature dependences of the specific heat below 5 K plotted as C/T vs. T^2 for different samples. A fit to the experimental data in the range below 4.5 K by using $C/T = \gamma + \beta T^2$ allows to estimate the values of the Sommerfeld coefficient γ related to the electronic contribution, and the prefactor β which characterizes the lattice contribution to the specific heat in a simple Debye approximation. For samples with non-superconducting behavior this procedure gives an estimate of γ in the normal state, γ_n, while for superconducting samples it yields the residual γ_r. The calculated values of these parameters are given in Table 4. For the oxygen-free bulky superconducting samples we obtained $\gamma_r = 0.82$–0.96 mJ/mol K^2. The obtained values of the residual γ_r for the oxygen-free superconducting samples are much lower than reported thus far by other authors for similar compositions [13,20,27]. These extremely low values of γ_r confirm the high purity of our oxygen-free samples. The obtained values of the residual γ_r for pure samples indicate that the volume fraction of the superconducting phase reaches $\sim$ 95–96% which agrees with the estimate obtained from the susceptibility data. A larger value of $\gamma_r = 5.2$ mJ/mol K^2 for sample Br N5 can be probably attributed to magnetic contribution from the Fe_3O_4 impurity although due to insulating nature of Fe_3O_4 at low temperatures one should not expect any contribution to γ_r. However, one cannot exclude, for example, the presence of glassy-like disorder in Fe_3O_4 with low energy excitations linear in temperature or additional magnetic excitations yielding a $T^{3/2}$ dependence of the specific heat. This problem needs additional study. For the samples with suppressed bulk superconductivity we obtained $\gamma_r = 19.3$ mJ/mol K^2. We also must note that the calculated values of the prefactor β for samples with high superconducting parameters and for those with reduced superconductivity are close to each other. This indicates that the electronic superconducting contribution to the specific heat in the range of temperatures used for fitting has only a minor influence and does not affect the accuracy of the calculations and hence, justifies the abovementioned fitting procedure and the correctness of the obtained parameters.

To get an additional independent estimate for the electronic and lattice contributions to the specific heat we used the following approach. For a description of the phonon spectrum a combined Einstein-Debye model was employed. The tetragonal unit cell of FeSe(Te) with space group P4/nmm contains two formula units giving rise to a total of 12 normal modes of vibrations. Their contribution was simulated by two Debye terms C_D and one Einstein term C_E with equal distribution of the spectral weight between the Debye and Einstein terms. These assumptions are in rough agreement with the results of the experimental study of the phonon density of states by nuclear inelastic scattering [28] and neutron scattering [29] on related $Fe_{1+x}Se$ superconductors.

The characteristic Debye and Einstein temperatures, Θ_D and Θ_E, were input parameters for a fit to the experimental temperature dependence of the total specific heat above T_c by the expression

$$C = C_{D1}(\Theta_{D1}) + C_{D2}(\Theta_{D2}) + C_E(\Theta_E) + \gamma_n T.$$

The fitting parameters were varied till the minimal deviations from a constant γ_n value in a maximal temperature range (up to 200 K) for the superconducting samples were achieved. The temperature dependence of the simulated lattice specific heat with these *optimized* values of $\Theta_{D1} = 127$ K, $\Theta_{D2} = 235$ K and $\Theta_E = 315$ K is shown by the dotted line in Figure 9. For the sample with suppressed bulk superconductivity by the dashed line Figure 9 also presents a curve calculated by subtracting the normal state electronic contribution $\gamma_n T$ (with $\gamma_n = 23$ mJ/mol K^2) from the measured total specific heat. At temperatures above 30 K both curves nicely

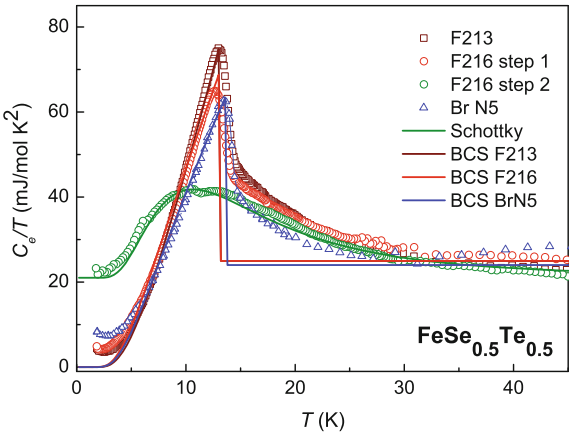

Fig. 11. (Color online) Temperature dependences of the electronic specific heat in representation C_e/T for different samples. The solid lines represent the fits describing, respectively, the superconducting specific heat for the bulk superconducting samples within the single-gap BCS model as given in the text, and the Schottky anomaly in the non-superconducting sample (F216 step 2).

coincide with deviations less than 2% in the complete temperature range up to 300 K. This consistency of the data again justifies the model used for the simulation of the phononic contribution. Note that no scaling of the phononic contribution for samples with high and low superconducting parameters was necessary. We found that the estimated values of the Sommerfeld coefficient in the normal state γ_n vary in the range 23–26 mJ/mol K^2 for different samples and are much lower than those reported previously for $FeSe_{1-x}Te_x$ by other authors [13,20,27]. To our opinion, the reason of this discrepancy is related to different estimates of the lattice contribution. In several earlier papers on FeSe(Te) a fit by an odd-power polynomial to the experimental data taken just above T_c was used to separate the electronic and lattice specific heat. Utilizing a similar fitting procedure for the temperature range 15–21 K we obtained for the normal electronic coefficient value $\gamma_n = 90$ mJ/mol K^2 and for the prefactor $\beta = 0.3$ mJ/mol K^4 corresponding to a Debye temperature $\Theta_D = 235$ K. However, the simple Debye approximation is known to work well only for temperatures below $\Theta_D/50 = 4.7$ K [30], which is much lower than the temperature range of fitting. Therefore these values of γ_n and Θ_D, are strongly overestimated. The failure of this extrapolation procedure was demonstrated recently also for the related superconducting $BaFe(Co)_2As_2$ pnictides [31].

The electronic specific heat C_e for all samples was determined by subtracting the calculated lattice contribution from the total measured specific heat. The dependences of the electronic specific heat in the representation C_e/T vs. T are shown in Figure 11 for different samples in a temperature range around the transition temperature. All samples with bulk superconductivity exhibit a sharp anomaly in C_e at T_c. The magnitude of the anomaly at T_c correlates with the amount of the superconducting phase in these samples. In the sample with suppressed superconducting properties no sharp anomaly at T_c is evidenced, but instead a broad cusp in C_e centered at around 10 K develops. A magnetic field of 90 kOe fully suppresses the residual filamentary superconductivity in this sample, as show the susceptibility measurements, but has a negligible effect on the specific heat. This suggests that the broad cusp in the electronic specific heat is not related to the superconducting behavior. Importantly, a part of this cusp-like anomaly is also evidenced in C_e for samples with bulk superconductivity as a broad right wing at temperatures above T_c. To check whether the broad cusp anomaly can be an artifact due to a possible incorrect description of the lattice specific heat at low temperatures, the contribution of the lowest phonon was varied up to the limiting value when it coincides with the total specific heat. However, even with this overestimated lattice contribution, the broad cusp in the electronic specific heat still remains present for all samples, although with somewhat reduced amplitude (by ∼20%) and with slight shift (by ∼1 K) to lower temperatures. These results indicate that the broad anomaly in the electronic specific heat is not an artifact due to an inadequate modeling of the phonon density of states, but is a feature reflecting the intrinsic properties of the studied samples. The typical Schottky-like appearance of this anomaly suggests an electronic origin, and the independence of magnetic field indicates its relation to the orbital degree of freedom. We speculate that it could originate from a splitting of the ground state of Fe^{2+} ions either by a crystal field or due to spin-orbital coupling. Therefore, this anomaly was simulated within a simple model of a two-level system. The results of the calculation are shown by a solid line for the sample with suppressed superconductivity using the data for a field of 90 kOe. We arrived at a reasonable description of the cusp at temperatures above 7 K with the value of the ground state splitting $\delta = 24$ cm^{-1} and the amount of magnetic species corresponding to ∼7% per mole. The only value that correlates with this quantity in our samples is the concentration of Fe ions on the 2c sites as resulting from the refinement of the X-ray data. As mentioned previously, these 2c site Fe ions can have a local magnetic moment. Therefore, it is natural to assume that they can also be responsible for the broad cusp-like anomaly in the electronic specific heat. However, the presence of this feature in the electronic specific heat in the samples with bulk superconductivity just above T_c indicates that the magnetic moment of these Fe ions is not the main factor that destroys superconductivity. A remarkably sharp behavior of the specific heat just below T_c and a strong dependence of the electronic specific heat on the magnetic field (see Fig. 12) observed for samples with bulk superconductivity along with extremely low values of their residual γ_r indicates that this contribution is fully suppressed in the superconducting state.

The temperature dependence of the electronic superconducting specific heat was analyzed within a BCS derived α-model [32,33] with a temperature dependent superconducting gap Δ, using a similar approach as described in reference [34] used for analysis of the specific

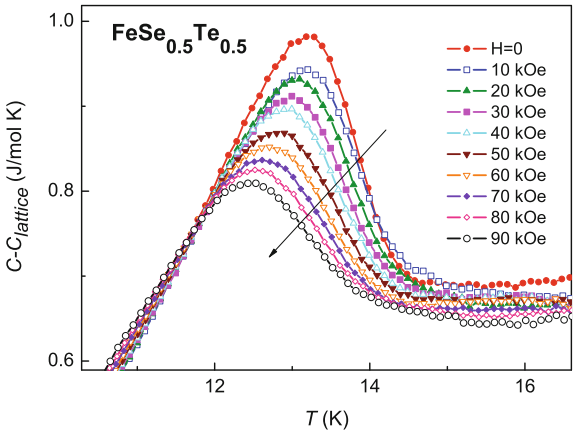

Fig. 12. (Color online) Temperature dependences of the electronic specific heat at different applied magnetic fields for oxygen-free sample F213 with bulk superconductivity. The arrow shows the direction of increasing field.

heat in related Ba(K)Fe_2As_2 pnictides. In Figure 11 fitting curves are shown by solid lines for three samples with high superconducting parameters. The fitting curves reasonably describe the superconducting specific heat, except in the range below 5 K which can be related to effects of residual impurities. The values of the superconducting gap at 0 K, Δ_0, derived from the analysis, vary within the range 26–28 K for different samples. The value of the coupling constant $2\Delta_0/T_c$ is close to the BCS value of 3.53.

We note that the obtained gap values $\Delta_0 = 2.4(1)$ meV are in good agreement with the value of 2.3 meV derived by Kato et al. [35] from scanning tunneling spectroscopy of $Fe_{1.05}Se_{0.15}Te_{0.85}$, by Homes et al. [36] from optical conductivity of $FeSe_{0.45}Te_{0.55}$, and with 2.6 meV obtained by Biswas et al. [37] from μSR, and by Bendele et al. [38] from magnetic penetration studies of $FeSe_{0.5}Te_{0.5}$. These studies and ARPES [39] indicate a multigap structure of $FeSe_{1-x}Te_x$. A fit to the electronic specific heat using a two-gap model, however, did not give an essential improvement compared to the single-gap model and therefore we conclude that the specific heat is dominated by only one gap of 2.4 meV.

Finally, in Figure 12 we present the data for variation of the superconducting specific heat under applied magnetic fields for one of the purest samples with high superconducting parameters. For better presentation the data are shown after subtracting the lattice contribution from the total specific heat. These dependences allow to get an estimate of the upper critical field H_{c2} from the temperature shift of the specific heat using the criterion of the minimum of the temperature derivative of C_e in the transition region. The respective dependence $H_{c2} = f(H)$ obtained from these data is shown by open squares in Figure 8. Interestingly, it exhibits a behavior resembling that of the H_{c2} curve determined from the resistivity data for the field applied along the *ab* plane. The calculations by the WHH formula [26] gave a value of $H_{c2}(0) \sim 980$ kOe which is by a factor of two larger than that obtained from the resistivity data. Similar results were recently reported for Ba(K)Fe_2As_2 pnictides by Popovich et al. [40], showing that $H_{c2}(0)$ derived from the specific heat is by a factor of two higher than that calculated from the resistivity, which was attributed to flux-flow effect due to vortex motion. We also would like to mention that concerning H_{c2} very similar data determined from specific heat and resistivity were recently reported by Serafin et al. [41], which were interpreted as due to the presence of strong thermal fluctuations in $FeSe_{0.5}Te_{0.5}$.

4 Concluding remarks

Our detailed studies of the structural, magnetic and thermodynamic properties of $FeSe_{0.5}Te_{0.5}$ reveal several important results:

(1) Preparation conditions have a substantial influence on the sample properties: the purity of the starting materials and handling atmosphere are crucial for obtaining high-purity samples. Samples prepared from the purified elements show superior properties compared to other cases. The oxygen-free samples prepared by fast cooling exhibit the lowest values of the susceptibility in the normal state, the highest transition temperature T_c^{on} of 14.4 K, contain a volume fraction of the superconducting phase up to 98%, and exhibit the most pronounced anomaly in the specific heat at T_c. In the oxygen-free samples prepared by slow cooling the bulk superconductivity is suppressed. They exhibit a paramagnetic tail in the susceptibility at low temperatures, a very small width of the hysteresis loop, and a strongly broadened resistive transition.

(2) The magnetic hysteresis measurements revealed high values of the critical current density j_c of 8.6×10^4 A/cm^2 for the purest samples which can be attributed to intrinsic inhomogeneity due to disorder at the anion sites. The oxidized samples show an increased j_c up to 2.3×10^5 A/cm^2 due to additional pinning centers of Fe_3O_4.

(3) The upper critical field H_{c2} of ~ 500 kOe is estimated from the resistivity study in magnetic fields parallel to the *c*-axis for both pure samples and samples containing oxide impurity. The anisotropy of the upper critical field $\gamma_{H_{c2}} = H_{c2}^{ab}/H_{c2}^{c}$ reaches a value of about 6 at $T/T_c = 0.996$ and is the highest reported to date for these materials.

(4) The specific-heat measurements evidenced very low values of the residual Sommerfeld coefficient corresponding up to 96% volume fraction of the superconducting phase which confirms the high quality of the oxygen-free samples. The value of the normal Sommerfeld coefficient $\gamma_n = 25$ mJ/mol K^2 obtained for pure samples is the lowest reported thus far for the $FeSe_{0.5}Te_{0.5}$.

(5) The temperature dependence of the electronic superconducting specific heat for samples with bulk superconductivity can be reasonably described within a single-band BCS model with the temperature dependent gap Δ_0 of value 27(1) K at $T = 0$ K. The values of

the coupling constant $2\Delta_0/T_c$ (see Tab. 3) are rather close to the BCS value of 3.53.

(6) The electronic specific heat of samples with suppressed bulk superconductivity shows a broad cusp-like anomaly which is ascribed to a splitting of the ground state of the Fe^{2+} ions at the 2c sites. This contribution is fully suppressed in the ordered state in samples with bulk superconductivity.

The authors thank Dana Vieweg and Nikola Pascher for experimental support. This research has been supported by the DFG via SPP 1458 and via Transregional Collaborative Research Center TRR 80 (Augsburg - Munich).

References

1. Y. Kamihara, T. Watanabe, M. Hirano, H. Hosono, J. Am. Chem. Soc. **130**, 3296 (2008)
2. M. Rotter, M. Tegel, D. Johrendt. Phys. Rev. Lett. **101**, 107006 (2008)
3. J.H. Tapp, Z. Tang, B. Lv, K. Sasmal, B. Lorenz, C.W. Chu, A.M. Guloy, Phys. Rev. B **78**, 060505 (2008)
4. F.-C. Hsu, J.Y. Luo, K.W. Yeh, T.K. Chen, T.W. Huang, P.M. Wu, Y.-C. Lee, Y.L. Huang, Y.-Y. Chu, D.C. Yan, M.-K. Wu, Proc. Natl. Acad. Sci. USA **105**, 14262 (2008)
5. J.W. Lynn, P. Dai, Physica C **469**, 469 (2009)
6. S. Li, C. de la Cruz, Q. Huang, Y. Chen, J.W. Lynn, J. Hu, Y.-L. Huang, F.-C. Hsu, K.-W. Yeh, M.-K. Wu, P. Dai, Phys. Rev. B **79**, 054503 (2009)
7. S. Medvedev, T.M. McQueen, I.A. Troyan, T. Palasyuk, M.I. Eremets, R.J. Cava, S. Naghavi, F. Casper, V. Ksenofontov, G. Wortmann, C. Felser, Nat. Mater. **8**, 630 (2009)
8. S. Margadonna, Y. Takabayashi, Y. Ohishi, Y. Mizuguchi, Y. Takano, T. Kagayama, T. Nakagawa, M. Takata, K. Prassides, Phys. Rev. B **80**, 064506 (2009)
9. T.M. McQueen, Q. Huang, V. Ksenofontov, C. Felser, Q. Xu, H. Zandbergen, Y.S. Hor, J. Allred, A.J. Williams, D. Qu, J. Checkelsky, N.P. Ong, R.J. Cava, Phys. Rev. B **79**, 014522 (2009)
10. E. Pomjakushina, K. Conder, V. Pomjakushin, M. Bendele, R. Khasanov, Phys. Rev. B **80**, 024517 (2009)
11. M.H. Fang, H.M. Pham, B. Qian, T.J. Liu, E.K. Vehstedt, Y. Liu, L. Spinu, Z.Q. Mao, Phys. Rev. B **78**, 224503 (2008)
12. K.W. Yeh, T.-W. Huang, Y. Huang, T.-K. Chen, F.-C. Hsu, P.M. Wu, Y.-C. Lee, Y.-Y. Chu, C.-L. Chen, J.-Y. Luo, D.-C. Yan, M.-K. Wu, Europhys. Lett. **84**, 37002 (2008)
13. B.C. Sales, A.S. Sefat, M.A. McGuire, R.Y. Jin, D. Mandrus, Y. Mozharivskyj, Phys. Rev. B **79**, 094521 (2009)
14. G.F. Chen, Z.G. Chen, J. Dong, W.Z. Hu, G. Li, X.D. Zhang, P. Zheng, J.L. Luo, N.L. Wang, Phys. Rev. B **79**, R140509 (2009)
15. R. Khasanov, M. Bendele, A. Amato, P. Babkevich, A.T. Boothroyd, A. Cervelino, K. Conder, S.N. Gvasaliya, H. Keller, H.-H. Klaus, H. Luetkens, V. Pomjakushin, E. Pomjakushina, B. Roessli, Phys. Rev. B **80**, R140511 (2009)
16. T. Taen, Y. Tsuchiya, Y. Nakajima, T. Tamegai, Phys. Rev. B **80**, 092502 (2009)
17. R. Hu, E.S. Bozin, J.B. Warren, C. Petrovic, Phys. Rev. B **80**, 214514 (2009)
18. J. Rodriguez-Carvajal, Physica B **192**, 55 (1993)
19. E.J.W. Verwey, Nature (London) **144**, 327 (1939)
20. T.J. Liu, X. Ke, B. Qian, J. Hu, D. Fobes, E.K. Vehstedt, H. Pham, J.H. Yang, M.H. Fang, L. Spinu, P. Schiffer, Y. Liu, Z.Q. Mao, Phys. Rev. B **79**, 174509 (2009)
21. B. Shen, P. Cheng, Z. Wang, L. Fang, C. Ren, L. Shan, H.-H. Wen, Phys. Rev. B **81**, 014503 (2010)
22. C.P. Bean, Phys. Rev. Lett. **8**, 250 (1962)
23. C.P. Bean, Rev. Mod. Phys. **36**, 90 (1964)
24. R. Prozorov, N. Ni, M.A. Tanatar, V.G. Kogan, R.T. Gordon, C. Martin, E.C. Blomberg, P. Prommapan, J.Q. Yan, S.L. Budko, P.C. Canfield, Phys. Rev. B **78**, 224506 (2009)
25. J. Yang, M. Matsui, M. Kawa, H. Ohta, C. Michioka, C. Dong, H. Wang, H. Yuan, M. Fang, K. Yoshimura, `arXiv:0911.4758` (unpublished)
26. N.R. Werthamer, E. Helfand, P.C. Hohenberg, Phys. Rev. **147**, 295 (1966)
27. B. Zeng, G. Mu, H.Q. Luo, T. Xiang, H. Yang, L. Shan, C. Ren, I.I. Mazin, P.C. Dai, H.-H. Wen, `arXiv:1007.3597` (unpublished)
28. V. Ksenofontov, G. Wortmann, A.I. Chumakov, T. Gasi, S. Medvedev, T.M. McQueen, R.J. Cava, C. Felser, Phys. Rev. B **81**, 184510 (2010)
29. D. Phelan, J.N. Millican, E.L. Thomas, J.B. Leao, Y. Qiu, R. Paul, Phys. Rev. B **79**, 014519 (2009)
30. C. Kittel, *Introduction to Solid State Physics* (John Wiley and Sons, Inc. New York, London, Sydney, Toronto 1971)
31. F. Hardy, T. Wolf, R.A. Fisher, R. Eder, P. Schweiss, P. Adelmann, H.V. Loehneysen, C. Meingast, Phys. Rev. B **81**, R060501 (2010)
32. F. Bouquet, Y. Wang, R.A. Fisher, D.G. Hinks, J.D. Jorgensen, A. Junod, N.E. Phillips, Europhys. Lett. **56**, 856 (2001)
33. H. Padamsee, J.E. Neighbor, C.A. Shiffman, J. Low Temp. Phys. **12**, 387 (1973)
34. Ch. Kant, J. Deisenhofer, A. Günther, F. Schrettle, A. Loidl, M. Rotter, D. Johrendt, Phys. Rev. B **81**, 014529 (2010)
35. T. Kato, Y. Mizuguchi, H. Nakamura, T. Machida, H. Sakata, Y. Takano, Phys. Rev. B **80**, R180507 (2009)
36. C.C. Homes, A. Akrap, J.S. Wen, Z.J. Xu, Z.W. Lin, Q. Li, G.D. Gu, Phys. Rev. B **81**, 180508 (2010)
37. P.K. Biswas, G. Balakrishnan, D.M. Paul, C.V. Tomy, M.R. Lees, A.D. Hillier, Phys. Rev. B **81**, 092510 (2010)
38. M. Bendele, S. Weyeneth, R. Puzniak, A. Maisuradze, E. Pomjakushina, K. Conder, V. Pomjakushin, H. Luetkens, S. Katrych, A. Wisniewski, R. Khasanov, H. Keller, Phys. Rev. B **81**, 224520 (2010)
39. F. Chen, B. Zhou, Y. Zhang, J. Wei, H.-W. Ou, J.-F. Zhao, C. He, Q.-Q. Ge, M. Arita, K. Shimada, H. Namatame, M. Taniguchi, Z.-Y. Lu, J. Hu, X.-Y. Cui, D.L. Feng, Phys. Rev. B **81**, 014526 (2010)
40. P. Popovich, A.V. Boris, O.V. Dolgov, A.A. Golubov, D.L. Sun, C.T. Lin, R.K. Kremer, B. Keimer, Phys. Rev. Lett. **105**, 027003 (2010)
41. A. Serafin, A.I. Coldea, A.Y. Ganin, M.J. Rosseinsky, K. Prassides, D. Vignolles, A. Carrington, Phys. Rev. B **82**, 104514 (2010)